The Astrophysical Journal, 673: L111–L114, 2008 February 1

WEAK-LENSING ELLIPTICITIES IN A STRONG-LENSING REGIME

Richard Massey[1] and David M. Goldberg[2]

Received 2007 September 10; accepted 2007 December 18; published 2008 January 8

ABSTRACT

It is now routine to measure the weak gravitational lensing shear signal from the mean ellipticity of distant galaxies. However, conversion between ellipticity and shear assumes local linearity of the lensing potential (i.e., that the spatial derivatives of the shear are small), and this condition is not satisfied in some of the most interesting regions of the sky. We extend a derivation of lensing equations to include higher order terms, and assess the level of biases introduced by assuming that first-order weak-lensing theory holds in a relatively strong shear regime. We find that even in a worst-case scenario, a fully linear analysis is accurate to within 1% outside ~1.07 times the Einstein radius of a lens, by deriving an analytic function that can be used to estimate the applicability of any first-order analysis. The effect is too small to explain the discrepancy between weak- and strong-lensing estimates of the mass of the Bullet Cluster, and should not impact cluster surveys for the foreseeable future. In fact, it means that arclets can be used to measure shears closer to a cluster core than has been generally appreciated. However, the bias is significant for galaxy group or galaxy-galaxy lensing applications. At the level of accuracy demanded by dedicated future surveys, it also needs to be considered for measurements of the inner slope of cluster mass distributions and the small-scale end of the mass power spectrum.

Subject heading: gravitational lensing

1. INTRODUCTION

Gravitational lensing is the deflection of light rays from a background light source by an intervening gravitational field (Mellier 1999; Refregier 2003). It is one of the most promising probes of the distribution of dark matter, and hence the effects of dark energy. Along lines of sight where the deflection is sufficient, "strong lensing" visibly distorts (and often multiply images) the shapes of individual background galaxies. However, only "weak lensing" is produced along most lines of sight, even those passing through the outskirts of galaxy clusters. This weaker but ubiquitous signal has to be collected statistically. To first order in a Taylor series, it is obtained from the mean ellipticity of an otherwise uncorrelated set of galaxies (Bartelmann & Schneider 2001).

Weak-lensing measurements have now been well used to map the distribution of mass (Clowe et al. 2006; Gavazzi & Soucail 2007; Massey et al. 2007b) and characterize its large-scale statistical properties (Massey et al. 2007a; Benjamin et al. 2007; Kitching et al. 2007). However, it is often the most massive structures that are of particular interest in the maps (e.g., Wittman 2005; Schirmer et al. 2007; Miyazaki et al. 2007) and that dominate the contribution to the power spectrum on small scales (e.g., Smith et al. 2003). Near such regions, the first-order assumptions implicit in a weak-lensing analysis no longer necessarily hold. In this Letter, we expand the Taylor series of the weak-lensing equation to include the next-highest terms, and investigate the level of bias in shear measurements that rely on simple measurements of ellipticity.

We derive the lensing equations in § 2. We check our results using ray-traced simulations in § 3, and we discuss their implications in § 4.

[1] California Institute of Technology, 1200 East California Boulevard, Pasadena, CA 91125.

[2] Department of Physics, Drexel University, 3141 Chestnut Street, Philadelphia, PA 19104.

2. LENSING TRANSFORMATIONS

2.1. *The Usual First-Order Treatment*

A general gravitational lens deflects light from position $\boldsymbol{x}'$ in a background (source) image to position $\boldsymbol{x}$ in the observed (lens) plane, such that

$$\boldsymbol{x}' = \boldsymbol{x} - \boldsymbol{\alpha}(\boldsymbol{x}), \tag{1}$$

where the deflection angle $\boldsymbol{\alpha}(\boldsymbol{x}) = \boldsymbol{\nabla}\Psi(\boldsymbol{x})$ is predicted by general relativity in the weak field limit, and $\Psi(\boldsymbol{x})$ is the Newtonian potential of the lens, $\Phi(\boldsymbol{x}, z)$, projected onto the plane of the sky.

Crucially, the gravitational field and the deflection angle vary across the sky. Assuming (the local linearity condition) that the change is linear on scales the size of a galaxy, it can be described to first order by a coordinate transformation

$$x_i' = x_i - \left(\frac{\partial\Psi}{\partial x_i}\right) - \frac{\partial}{\partial x_j}\left(\frac{\partial\Psi}{\partial x_i}\right)\Delta x_j + \cdots . \tag{2}$$

The first derivative term represents an unmeasurable centroid shift. Placing the origin of the coordinate system at the galaxy's observed center of light, we are left with

$$x_i' = \mathcal{A}_{ij} x_j + \cdots , \tag{3}$$

where the Jacobian of the transformation is

$$\mathcal{A}_{ij} = \delta_{ij} - \frac{\partial^2\Psi}{\partial x_i \partial x_j}, \tag{4}$$

$$\mathcal{A} \equiv \begin{pmatrix} 1-\kappa-\gamma_1 & -\gamma_2 \\ -\gamma_2 & 1-\kappa+\gamma_1 \end{pmatrix}. \tag{5}$$

We have introduced the usual notation of convergence

$\kappa(\boldsymbol{x}) \equiv \boldsymbol{\nabla}^2\Psi(\boldsymbol{x})/2$, and two components of shear $\gamma_i(\boldsymbol{x})$. The inverse mapping is simply

$$x_i = (\mathcal{A})^{-1}_{ij} x'_j + \cdots . \tag{6}$$

The shape of a galaxy image $I(x')$ can be quantified via its intrinsic ellipticity

$$\{\chi_1^{\rm int},\, \chi_2^{\rm int}\} \equiv \left\{ \frac{Q_{11}^{\rm int} - Q_{22}^{\rm int}}{Q_{11}^{\rm int} + Q_{22}^{\rm int}},\ \frac{2Q_{12}^{\rm int}}{Q_{11}^{\rm int} + Q_{22}^{\rm int}} \right\}, \tag{7}$$

where its quadrupole moments are

$$Q_{ij}^{\rm int} \equiv \frac{\int I(\boldsymbol{x}') x'_i x'_j d^2\boldsymbol{x}'}{\int I(\boldsymbol{x}') d^2\boldsymbol{x}'}. \tag{8}$$

Under the (locally linear) lensing transformation (6), the galaxy's observed ellipticity becomes

$$\chi_i^{\rm lin} = \chi_i^{\rm int} + 2\gamma_i - \chi_i^{\rm int}(\chi_j^{\rm int}\gamma_j) + \cdots \tag{9}$$

to first order in γ (Seitz & Schneider 1995). Averaging over a population of galaxies with uncorrelated intrinsic shapes $\langle \chi^{\rm int} \rangle = 0$, an estimator $\tilde{\gamma}$ can then recover the gravitational shear signal

$$\langle \tilde{\gamma}_i \rangle \equiv \frac{\langle \chi_i^{\rm lin} \rangle}{2 - \langle (\chi_i^{\rm int})^2 \rangle} = \langle \gamma_i \rangle + O(\gamma^2). \tag{10}$$

The variance in the denominator can be closely approximated by the observed value, which is typically ~0.4 (Leauthaud et al. 2007).

For practical purposes, a weight function $W(\boldsymbol{x})$ with finite support is also usually applied to the integrals in equation (8). This complicates the shear estimator: the shear polarizability tensor P^γ in Kaiser et al. (1995), which generalizes the denominator of equation (10), involves derivatives of $W(\boldsymbol{x})$. However, P^γ is typically fitted from a large ensemble of galaxy shapes to reduce noise, and almost all of those galaxies will be on lines of sight unaffected by higher order lensing terms. We therefore ignore the effect here.[3]

2.2. *Higher Order Terms*

Continuing the Taylor series in equation (2), we can write (cf. Goldberg & Natarajan 2002)

$$x'_i = \mathcal{A}_{ij} x_j - \frac{1}{2}\frac{\partial^3\Psi}{\partial x_i \partial x_j \partial x_k} x_j x_k - \frac{1}{6}\frac{\partial^4\Psi}{\partial x_i \partial x_j \partial x_k \partial x_l} x_j x_k x_l + \cdots . \tag{11}$$

Repeatedly substituting the simple form

$$x_i = (\mathcal{A})^{-1}_{ij}\left(x'_j + \frac{1}{2}\Psi_{,jkl}\, x_k x_l + \frac{1}{6}\Psi_{,jklm}\, x_k x_l x_m \right) \tag{12}$$

into itself then yields the inverse mapping

$$\begin{aligned} x_i = {} & (\mathcal{A})^{-1}_{ij} x'_j \\ & + \frac{1}{2}(\mathcal{A})^{-1}_{ij}(\mathcal{A})^{-1}_{kp}(\mathcal{A})^{-1}_{lq}\Psi_{,jkl} x'_p x'_q \\ & + \frac{1}{6}(\mathcal{A})^{-1}_{ij}(\mathcal{A})^{-1}_{kp}(\mathcal{A})^{-1}_{lq}(\mathcal{A})^{-1}_{mr}\Psi_{,jklm} x'_p x'_q x'_r \\ & + \frac{1}{2}(\mathcal{A})^{-1}_{ij}(\mathcal{A})^{-1}_{kp}(\mathcal{A})^{-1}_{lm}(\mathcal{A})^{-1}_{nq}(\mathcal{A})^{-1}_{sr} \\ & \times \Psi_{,jkl}\Psi_{,mns} x'_p x'_q x'_r + \cdots . \end{aligned} \tag{13}$$

The various terms are listed in order of decreasing importance. Third derivatives of Ψ are related to the *flexion* signal (Goldberg & Bacon 2005; Bacon et al. 2006). This is small for realistic potentials; higher derivatives of Ψ will be smaller still. Note that this relation still holds locally even if there are multiple images, but that there will be different values of $\mathcal{A}$ at each image.

To complicate matters, this mapping now shifts the galaxy's center of light by less than $\boldsymbol{\alpha}$. If the coordinate system were located as in the linear case, the observed centroid would now be

$$\langle x_i \rangle \approx \frac{1}{2}(\mathcal{A})^{-1}_{ij}(\mathcal{A})^{-1}_{km}(\mathcal{A})^{-1}_{ln}\Psi_{,jkl} Q^{\rm int}_{mn}, \tag{14}$$

plus smaller contributions coming from the galaxy's intrinsic octopole moment. In a coordinate system centered on the observed image, the mapping (for a fully general potential) is therefore (cf. eq. [6])

$$\begin{aligned} x_i = {} & (\mathcal{A})^{-1}_{ij} x'_j \\ & + \frac{1}{2}(\mathcal{A})^{-1}_{ij}(\mathcal{A})^{-1}_{kp}(\mathcal{A})^{-1}_{lq}\Psi_{,jkl}\left(x'_p x'_q - Q^{\rm int}_{pq} \right) \\ & + \frac{1}{6}(\mathcal{A})^{-1}_{ij}(\mathcal{A})^{-1}_{kp}(\mathcal{A})^{-1}_{lq}(\mathcal{A})^{-1}_{mr}\Psi_{,jklm} x'_p x'_q x'_r \\ & + \frac{1}{2}(\mathcal{A})^{-1}_{ij}(\mathcal{A})^{-1}_{kp}(\mathcal{A})^{-1}_{lm}(\mathcal{A})^{-1}_{nq}(\mathcal{A})^{-1}_{sr} \\ & \times \Psi_{,jkl}\Psi_{,mns} x'_p x'_q x'_r + \cdots . \end{aligned} \tag{15}$$

In practice, a galaxy's intrinsic quadrupole moments cannot be observed. We could expand them as a function of the galaxy's observed shape using equation (11). However, several non-negligible coefficients produce an unwieldly general expression.

To make the equations more tractable, we now fix various properties of the lens. It is always possible to adopt an arbitrary choice of rotation for the coordinate system such that $\Psi_{,12} = 0$ (so $\mathcal{A}$ is diagonal), and invoke parity symmetry to consider only that the potential increases to the right (hence $\gamma_1 < 0$). We also work only in the "positive parity" lensing regime (outside the critical curve), where $\det\mathcal{A} > 0$. Our analysis is equally valid inside the critical curve, but breaks down if a part of the image crosses the critical curve (cf. Schneider & Er 2007). We additionally approximate as zero all derivatives of Ψ that are "odd" at 90° ($\Psi_{,112}$, $\Psi_{,222}$, $\Psi_{,1112}$, and $\Psi_{,1222}$). This is explicitly

[3] As pointed out during the derivation of "reduced shear" by Bartelmann & Schneider (2001) a galaxy's flux $I(\boldsymbol{x}')$ could be replaced in eq. (8) and throughout by a monotonic function of intensity $f(I(\boldsymbol{x}'))$, without any change in the formalism. This approximates a useful weighting scheme.

true for a circular potential or at the major and minor axes of an elliptical potential.

Since we are in a fairly strong lensing regime, it is not unreasonable to also assume that $\gamma \gg \chi^{\rm int}$, so the source galaxy can be considered intrinsically circular. It still has a size $R^2 \equiv 2Q_{11}^{\rm int} = 2Q_{22}^{\rm int}$ and concentration index

$$c \equiv \frac{\int I(\boldsymbol{x})|\boldsymbol{x}|^4 d^2\boldsymbol{x}}{(R^2)^2 \int I(\boldsymbol{x}) d^2\boldsymbol{x}}, \tag{16}$$

which is 2 for a Gaussian, 10/3 for an exponential, and higher for a de Vaucouleurs profile.

The observed ellipticity then simplifies to

$$\begin{aligned}\chi_1^{\rm obs} = \chi_1^{\rm lin} - \frac{a^2 d^2 R^2}{4(a^2+d^2)^2}\{&(a^2\Psi_{,111} + d^2\Psi_{,122})^2 \\ &- c[15a^4\Psi_{,111}^2 - (12a^2d^2 + 4ad^3 - 3d^4)\Psi_{,122}^2 \\ &- 2a^2d(2a-3d)\Psi_{,111}\Psi_{,122} \\ &+ 4a^3\Psi_{,1111} - 4ad(a-d)\Psi_{,1122} - 4d^3\Psi_{,2222}]\}. \end{aligned} \tag{17}$$

where $a \equiv (\mathcal{A}^{-1})_{11} = (1 - \Psi_{,11})^{-1}$ and $d \equiv (\mathcal{A}^{-1})_{22} = (1 - \Psi_{,22})^{-1}$ are unitless. For a singular isothermal sphere (SIS) lens, $\Psi(\boldsymbol{x}) = \theta_{\rm E}|\boldsymbol{x}|$,

$$\chi_1^{\rm obs} = \chi_1^{\rm lin} + \frac{cR^2}{\theta_{\rm E}^2}\,\frac{4r^3 - (9 + 1/c)r^2 + 12r - 4}{4(r-1)^2(2r^2 - 2r + 1)^2}, \tag{18}$$

where $r \equiv |\boldsymbol{x}|/\theta_{\rm E}$ and $\chi_1^{\rm lin} = (1 - 2r)/(2r^2 - 2r + 1)$.

3. VERIFICATION THROUGH RAY-TRACING

We have developed a simple ray-tracing routine to deflect rays via equation (1), deforming the shapes of source galaxies into arcs. Figure 1 shows the apparent ellipticity of an intrinsically circular Gaussian source with width σ, when seen behind a singular isothermal sphere lens with Einstein radius $\theta_{\rm E}$. The two examples, with $\sigma/\theta_{\rm E} = 0.006$ and 0.12, illustrate a median-sized $i' = 25$ galaxy (Leauthaud et al. 2007) at $z = 1$ behind cluster Abell 1689, in which $\theta_{\rm E} = 45''$ (Clowe & Schneider 2001), and behind a more modest galaxy group. The Bullet Cluster is not spherical, but has a mean Einstein radius of $\sim 35''$ for the main and $\sim 30''$ for the secondary peak (M. Bradač 2007, private communication).

The ray-tracing calculation and all analytic models converge at large distances from the lens. However, while ellipticity increases monotonically toward the Einstein radius under the assumption of local linearity, in more realistic calculations, image curvature due to higher order terms reduces the measured ellipticity. Very close to the Einstein radius, our second-order model 17 overestimates the deviation from a linear model compared to ray-traced measurements due to even higher order terms. It thus represents a worst-case scenario.

4. DISCUSSION

We have derived the next-highest terms in the coordinate transformation relevant for weak gravitational lensing, by dropping the assumption of "local linearity," which acts as a useful constraint on the applicability of the linear approximation. The resulting equations are not elegant, but can be simplified by making several reasonable assumptions about the galaxy's intrinsic shape and the lens profile. We provide a convenient formula in the case of a singular isothermal sphere lens. As expected, the perturbations from linear lensing theory are greatest for large galaxies; they increase as the size of the galaxy squared. As with gravitational flexion, this is simply due to the accumulating change in shear signal across the width of a galaxy image.

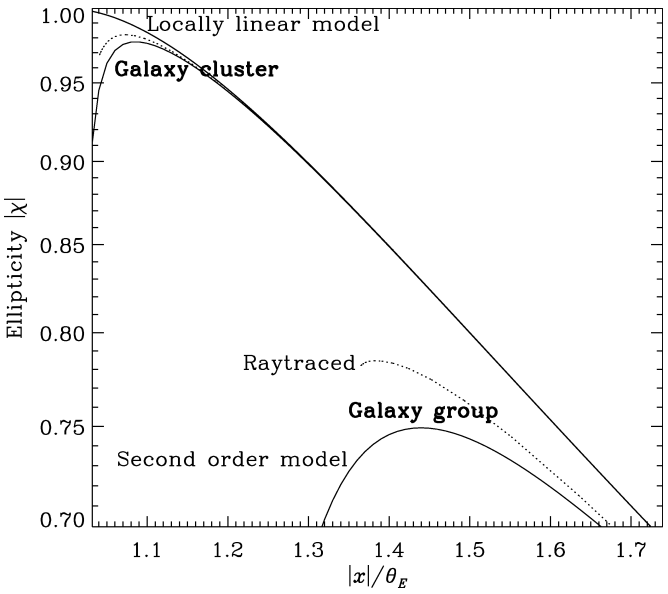

FIG. 1.—Observed ellipticity of an intrinsically circular galaxy with a Gaussian radial profile, seen at various radii behind a singular isothermal sphere lens. The two groups of curves represent the cases of a typical galaxy cluster lens and a galaxy group lens. In both, the solid lines depict analytic models: with the assumption of local linearity (these produce the same curve) and including second-order terms. The dotted lines show measured values from a fully ray-traced simulation.

A linear lensing analysis systematically overestimates the shear signal near an Einstein radius. However, it is negligible for galaxy cluster lenses surprisingly far into the nonlinear regime. Assuming a value of 1.6 for the denominator of equation (10), the linear approximation is within 1% of the true shear outside $\sim 1.07\theta_{\rm E}$, where $\gamma \approx 0.47$, and the reduced shear, $g \approx 0.93$. Compared to other potential errors in immediately forthcoming surveys, we therefore conclude that this will be of only minor concern for measurements of the mass of individual (or even stacked) clusters. For example, the effect is in the right direction but an order of magnitude too small to explain the discrepancy between measurements of the mass in the Bullet Cluster (Clowe et al. 2006) via strong and weak lensing. However, the effect ought to be considered by measurements of the inner slopes of cluster mass distributions or the mass power spectrum on small scales. It is also more immediately significant for mass measurements of galaxy groups and galaxy-galaxy lensing.

We have not investigated the correction for a point-spread function or the use of a weight function while measuring galaxy shapes. A full analysis of these would be interesting in future work.

The authors thank Maruša Bradač, Douglas Clowe, Yannick Mellier, Barnaby Rowe, and an anonymous referee. This work was supported by NASA grant ATP04-0000-0067 and DoE grant FG02-04ER41316.

REFERENCES

Bacon, D., Goldberg, D., Rowe, B., & Taylor, A. 2006, MNRAS, 365, 414
Bartelmann, M., & Schneider, P. 2001, Phys. Rep., 340, 291
Benjamin, J., et al. 2007, MNRAS, 381, 702
Clowe, D., Bradac, M., Gonzalez, A., Markevitch, M., Randall, S., Jones, C., & Zaritsky, D. 2006, ApJ, 648, L109
Clowe, D., & Schneider, P. 2001, A&A, 379, 384
Gavazzi, R., & Soucail, G. 2007, A&A, 462, 459
Goldberg, D., & Bacon, D. 2005, ApJ, 619, 741
Goldberg, D., & Natarajan, P. 2002, ApJ, 564, 65
Kaiser, N., Squires, G., & Broadhurst, T. 1995, ApJ, 449, 460
Kitching, T., Heavens, A., Taylor, A., Brown, M., Meisenheimer, K., Wolf, C., Gray, M., & Bacon, D. 2007, MNRAS, 376, 771
Leauthaud, A., et al. 2007, ApJS, 172, 219
Massey, R., et al. 2007a, ApJS, 172, 239
———. 2007b, Nature, 445, 286
Mellier, Y. 1999, ARA&A, 37, 127
Miyazaki, S., Hamana, T., Ellis, R. S., Kashikawa, N., Massey, R. J., Taylor, J., & Refregier, A. 2007, ApJ, 669, 714
Refregier, A. 2003, ARA&A, 41, 645
Schirmer, M., Erben, T., Hetterscheidt, M., & Schneider, P. 2007, A&A, 462, 875
Schneider, P., & Er, X. 2007, A&A, submitted (arXiv:0709.1003)
Seitz, S., & Schneider, P. 1995, A&A, 294, 411
Smith, R., et al. 2003, MNRAS, 341, 1311
Wittman, D. 2005, ApJ, 632, L5